Springer

Journal of Mechanical Science and Technology 23 (2009) 3424~3435

Journal of Mechanical Science and Technology

www.springerlink.com/content/1738-494x
DOI 10.1007/s12206-009-1017-9

Numerical simulation of structure and no formation of turbulent lean-premixed flames in gas turbine conditions †

Sungmo Kang, Yongmo Kim* and Kwan-Soo Lee

Department of Mechanical Engineering, Hanyang University, Seoul, 133-791, South Korea

(Manuscript Received February 20, 2009; Revised August 24, 2009; Accepted August 28, 2009)

Abstract

This study numerically investigates the detailed structure and NO formation in atmospheric and high-pressure lean-premixed flames. Parallel unstructured-grid finite-volume method (FVM) has been developed to maintain the geometric flexibility and computational efficiency for the solution of the physically and geometrically complex flows. In order to realistically represent the complex turbulence-chemistry interaction of high-pressure lean-premixed turbulent flames encountered in gas turbine combustors, a flamelet model based on the level-set approach has been adopted. Special emphasis is given to the effects of pressure and equivalence ratio on the flame front location and NO formation, as well as the dimensionless parameters including turbulent Reynolds number, Re, Damköhler number, Da, and Karlovitz number, Ka in the lean-premixed gas turbine-like situations. Numerical results obtained in this study suggest that the level-set approach in the context of parallel unstructured-grid FVM is capable of realistically simulating the detailed structure and NO formation in the atmospheric and high-pressure lean-premixed flames.

Keywords: Flame structure; High-pressure lean mixture; Level-set approach; NOx formation; Turbulent premixed flame

1. Introduction

Most of the low-NOx power-generation gas turbines operate in lean-premixed mode because this reduces the flame temperature and substantially decreases the NO emission. However, as the equivalence ratio decreases towards the lean flammability limit, the combustion process becomes susceptible to flame instabilities such as flashback and blowout. In lean-premixed gas turbine engines, turbulence-chemistry interaction is much stronger and combustion could occur at the thin reaction zone or broken reaction zone. To ensure the flame stabilization, the design concept of the lean-premixed dry low emission (DLE) combustors is quite different from one of the conventional nonpremixed combustors. For the flame stabilization of the lean-premixed combustors, a significant degree of the flow-induced swirl is usually required to achieve the flow reversal through vortex breakdown. Thus, a large portion of the air is swirled to stabilize the lean-premixed combustion processes. In the swirl-induced recirculation zone, the flame-holding process is achieved by continuously providing the ignition source through the mixing of hot combustion products with the incoming unburned mixture. This flame stabilization process utilizing the flow recirculation creates the low fluid-particle velocity region together with sufficiently long residence time and the high turbulence intensities which are essentially needed for the flame anchoring in the turbulent reacting flow processes of the gas turbine combustors. In this aspect, the combustion model must have a capability to realistically simulate this detailed structure, the NO formation, and the flame stabilization processes.

† This paper was recommended for publication in revised form by Associate Editor Ohchae Kwon

* Corresponding author. Tel.: +82 2220 0428, Fax.: +82 2 2297 0339
E-mail address: ymkim@hanyang.ac.kr

The high-pressure lean-premixed flames of lean-premixed gas turbine combustors are characterized by high turbulent Reynolds number, low Damköhler number, and high Karlovitz number. According to Borghi's diagram [1], the combustion regime of the lean-premixed gas turbine combustors can be classified as the distributed reaction regime in which the smallest turbulent eddies are thinner than the thickness of the reaction front. However, recently, Peters refined this distributed reaction zone as the thin reaction zone and the broken reaction zone [2]. The condition of the thin reaction zone is defined by Re > 1.0 and 1.0 < Ka < 100. In the thin reaction zone, the preheat zone is thicker than the size of the smallest turbulent eddy and an inner reaction layer is thinner than Kolmogorov eddies. This implies that, in this thin reaction zone, the smallest turbulent eddies can interact strongly with the thick preheat zone, but they are unable to penetrate the thin reaction layer.

In general, the comprehensive numerical model for analyzing the combustion processes of gas turbine engines must deal with the premixed, partially premixed, and nonpremixed flame fields. In dealing with the nonpremixed turbulent flames, the reliable and robust combustion models including the laminar flamelet concept [3] and the conditional moment closure [4] have been well developed. However, many combustion models for turbulent premixed or partially-premixed flames were not quite successful for the design analysis of combustors due to their complexities and limitations. So far, an ad-hoc approach like the eddy dissipation model is quite often applied to the industrial design analysis. The more advanced models include a strained premixed flamelet model [5], a turbulent flame speed closure [6], and a level-set-based flamelet model [7]. Among these turbulent combustion models, the level-set-based flamelet model suggested by Chen et al. [7] has the capability to realistically simulate turbulent premixed and partially-premixed flames with numerical efficiency and robustness. The level-set-based flamelet model uses the two scalar fields, $G(\boldsymbol{x}, t)$, which determines the location of premixed flame front and $Z(\boldsymbol{x}, t)$, which expresses the state of mixing in turbulent partially-premixed flame. This requires a formulation for both premixed and non-premixed combustion. Since the level-set approach is applicable to simulate the thin reaction zone frequently encountered in the flame fields of the lean-premixed gas turbine engine as well as the partially-premixed combustion situations, this approach has been adopted in the present study.

Atmospheric [8] and high-pressure [9] turbulent lean-premixed Bunsen flames are chosen as validation cases. Based on numerical results, detailed discussions have been made for the flame structure and NOx formation in the high-pressure lean-premixed turbulent flames.

2. Physical and numerical models

2.1 Governing equations

For the turbulent reacting flows involving a number of species N, Favre-averaged [10] equations for the Navier-Stokes system, the standard k-ε turbulence model, and the mean and the variance of mixture fraction are employed and represented in a Cartesian tensor form:

$$\frac{\partial}{\partial t}(\bar{\rho}\tilde{\phi})+\frac{\partial}{\partial x_j}(\bar{\rho}\tilde{u}_j\tilde{\phi})=\frac{\partial}{\partial x_j}\left(\Gamma_\phi\frac{\partial\tilde{\phi}}{\partial x_j}\right)+S_\phi \tag{1}$$

where ϕ includes velocity vector (u_i), static enthalpy (h), turbulent kinetic energy (k), dissipation rate (ε), mixture fraction (Z), and variance (Z''^2). Γ_ϕ and S_ϕ represent the diffusion coefficient and the source term of its equation, respectively. Diffusion coefficients and source terms can be found in our previous work [11]. As an alternative to local equivalence ratio, the mean mixture fraction is solved for to account for changes in the local equivalence ratio due to entrainment of air and/or different equivalence ratios among incoming mixtures. To account for heat losses due to radiation and air-/water-cooling at the wall, the mean enthalpy equation is solved. The convective heat transfer at the wall is treated using the conventional wall-function approach, and a radiative heat-loss rate is modeled by the optically-thin radiation model [12]. The mean temperature is calculated from the mean enthalpy ($\tilde{h}$) by using local mean mass fractions ($\tilde{Y}_i$) and then, the density is determined from the equation of state under low-Mach number assumption:

$$\sum_{i=1}^{\mathrm{N}}\tilde{Y}_i h_i(\tilde{T})=\tilde{h}(x,t) \text{ and } h_i=\mathrm{h}_i^0+\int_{T^0}^{\tilde{T}}c_{pi}(\tilde{T})\mathrm{d}T \tag{2}$$

$$\bar{\rho}=\frac{p_0 W}{\mathrm{R}^0\tilde{T}} \text{ and } \frac{1}{W}=\sum_{i=1}^{\mathrm{N}}\frac{\tilde{Y}_i}{W_i} \tag{3}$$

where h_i^0 is the standard heat of formation per unit mass for species i at reference temperature T^0, c_p the specific heat, p_0 the ambient thermodynamic pressure, R^0 the universal gas constant with the value 8.31434 J mole^{-1} K^{-1}, and W the local effective molar mass of the mixture. The mean mass fractions are calculated using the presumed-shape pdf (probability density function) approach which will be presented in Sec.2.3.

2.2 Level-set G-based flamelet model

In the turbulent partially-premixed flames, a formulation for both premixed and nonpremixed combustion has to be used. For this purpose, according to the point of view, the flamelet model for non-premixed combustion could be combined with the flamelet model for premixed combustion, and vice versa. However, the mixing of fuel and oxidizer in the turbulent flow field is usually described by the transport equations for the mean and the variance of mixture fraction.

To describe premixed combustion, the level-set approach [13] based on the G-equation [14] is introduced, where an iso-scalar surface $G(\boldsymbol{x}, t)=G_0$ defines the location of the instantaneous premixed flame front. Thus, this surface divides the flow field into two regions: burnt gas where $G(\boldsymbol{x}, t) > G_0$ and unburnt mixture where $G(\boldsymbol{x}, t) < G_0$. Since G is a nonreacting scalar, it avoids complications associated with counter-gradient diffusion and there is no need for a source term closure. The equation for the mean location of the turbulent flame front is written as [3]

$$\frac{\partial(\overline{\rho}\tilde{G})}{\partial t}+\nabla\bullet(\overline{\rho}\tilde{u}\tilde{G})=(\overline{\rho}s_T)|\nabla\tilde{G}|-\overline{\rho}D_t\tilde{\kappa}|\nabla\tilde{G}| \quad (4)$$

$$\tilde{\kappa}=\nabla\bullet\tilde{n}=\nabla\bullet\left(-\frac{\nabla\tilde{G}}{|\nabla\tilde{G}|}\right) \quad (5)$$

where s_T is the turbulent burning velocity, $\tilde{\kappa}$ the curvature of the mean flame front, $\tilde{n}$ the unit vector normal to the mean flame front, and D_t the turbulent diffusivity, which can be determined from the integral length scale l and the velocity fluctuation u' as

$$D_t=a_4 l u',\ \ l=a_1 u'^3/\tilde{\varepsilon},\ \ u'=(\tilde{k}/a_2)^{1/2} \quad (6)$$

where the constants are a_1=0.37, a_2=1.5, and a_4=0.78 [3]. The equation for the variance of $\tilde{G}$ is [3]

$$\frac{\partial(\overline{\rho}\widetilde{G''^2})}{\partial t}+\nabla\bullet(\overline{\rho}\tilde{u}\widetilde{G''^2}) =\nabla_{\|}\bullet(\overline{\rho}D_t\nabla_{\|}\widetilde{G''^2})+2\overline{\rho}D_t(\nabla\tilde{G})^2-c_s\overline{\rho}\frac{\tilde{\varepsilon}}{\tilde{k}}\widetilde{G''^2} \quad (7)$$

where c_s is a modeling constant of 2.0. The tangential diffusion operator may be calculated by subtracting the normal diffusion from the diffusive operator as [3]

$$\nabla_{\|}\bullet(\overline{\rho}D_t\nabla_{\|}\widetilde{G''^2})=\nabla\bullet(\overline{\rho}D_t\nabla\widetilde{G''^2})-\tilde{n}\bullet\nabla(\overline{\rho}D_t\tilde{n}\bullet\nabla\widetilde{G''^2}) \quad (8)$$

For premixed turbulent combustion, s_T can be determined from an algebraic correlation [3]:

$$\frac{s_T-s_L}{u'}=-\frac{a_4b_3^2}{2b_1}\mathrm{Da}+\left[\left(\frac{a_4b_3^2}{2b_1}\mathrm{Da}\right)^2+a_4b_3^2\mathrm{Da}\right]^{1/2} \quad (9)$$

where s_L is the laminar burning velocity of a plane flame, the Damköhler number is $\mathrm{Da}=s_L l/(u' l_F)$, l_F is the laminar flame thickness, and the constants are b_1=2.0 and b_3=1.0. For the partially-premixed flame propagation through a stratified, locally premixed environment, a conditional turbulent Damköhler number Da(Z) as a function of the mixture fraction (Z) is introduced to determine the conditional turbulent burning velocity $s_T(Z)$ as

$$s_T(Z)=s_L(Z)+u' f\{\mathrm{Da}(Z)\} \quad (10)$$

where $f\{\mathrm{Da}\}$ represents the right-hand side of Eq. (9) and Da (Z) is defined as [3]

$$\mathrm{Da}(Z)=\frac{s_L(Z)l}{u' l_F(Z)}=\frac{s_L^2(Z)l}{u'D} \quad (11)$$

In the second equality in the above equation, the laminar flame thickness is replaced by $l_F(Z)=D/s_L(Z)$. The laminar thermal diffusivity D is assumed mixture fraction independent, defined as [3]

$$D=(\lambda/c_p)_\delta/\rho_u \quad (12)$$

where the heat conductivity λ and the heat capacity c_p are evaluated at the inner layer temperature T_δ and ρ_u is the unburnt mixture density. Thus D is dependent on the operating pressure p_0 and temperature T_0, by which describes the pressurized and preheating effects.

2.3 Flamelet library and presumed-shape pdf approach

By solving flamelet equations, flamelets are generated and tabulated into the flamelet library, so called, which is preprocessed prior to flow calculations. For species i, a laminar flamelet library is denoted by Y_i (x_n, ϕ, ζ). Here, ζ denotes the defect from adiabatic enthalpy, ϕ the equivalence ratio, and $x_n=(G-G_0)/\sigma$ the flamelet normal coordinate, whose origin $G=G_0$ is fixed at the inner layer. This study defines it at the peak of CH2O concentration. Assuming that the normal distance to the mean flame front is $\widetilde{x_n} = (\tilde{G}(x) - G_0)/\tilde{\sigma}$ and $\tilde{G}$ is the Favre mean in space, the mean mass fraction of species i may be calculated as

$$\widetilde{Y_i}(x) = \int_{-\infty}^{0}\int_{0}^{+\infty}\int_{-\infty}^{+\infty} Y_i(x_n,\phi,\zeta)P(x_n,\phi,\zeta;x)\mathrm{d}x_n\mathrm{d}\phi\mathrm{d}\zeta \tag{13}$$

Here the flame surface area ratio is approximated as $\tilde{\sigma} = s_T / s_L$. The joint pdf $P(x_n, \phi, \zeta)$ can be obtained in different ways such as measurements or a pdf-transport formulation [15] but more often a presumed-shape pdf approach is used [3,16,17]. Using Bayes' theorem and assuming the stochastic random variables being statistically independent leads to

$$P(x_n,\phi,\zeta) = P(x_n)\,P(\phi)\,P(\zeta) \tag{14}$$

The joint pdf can be obtained if $P(x_n)$, $P(\phi)$, and $P(\zeta)$ are modeled separately. Here Gaussian shape is assumed for the marginal pdf $P(x_n)$ [18]:

$$P(x_n) = (2\pi\widetilde{x_n''^2})^{-1/2}\exp[-(x_n-\widetilde{x_n})^2/(2\widetilde{x_n''^2})] \quad \text{with} \quad \widetilde{x_n''^2} = \widetilde{G''^2}/\tilde{\sigma}^2 \tag{15}$$

The delta function is used for $P(\phi)$ under the assumption that it can be a choice for the premixed flames which have the dominant premixed combustion mode and the relatively low gradient of mixture fraction in the main flame zone. Similarly, the shape of $P(\zeta)$ is taken as a delta function with neglect of its fluctuations.

To account for heat losses due to convective and radiative heat transfer, this study adopts an enthalpy-defect concept used for nonpremixed combustion [19] as well as a nonadiabatic premixed flamelet model suggested in FPI method [20]. Fig. 1 shows the typical laminar premixed methane/air flames from adiabatic level to quenching for two pressures (p_0=5, 10 bar; ϕ=0.5, T_0=673 K). The result shows the nonadiabatic effect on temperature and OH radical.

Here, all 1-D laminar premixed flames and thermodynamic properties are computed by the CHEMKIN-II package [21], using chemical kinetics based on the GRI-Mech 3.0 involving 53 species and 325-elementary reactions [22].

2.4 Post-processing step for NOx formation

The steady flamelet model inevitably predicts the NOx formation through a post-processing step which requires the additional modeling of NOx formation rates. For the lean-premixed methane/air flame, NOx formation is mainly due to N2O mechanism, Fenimore prompt-NO mechanism, and Zeldovich thermal-NO mechanism. A model for these three pathways for NO formation has been proposed and well documented in a recent work, where the NO model is integrated into a radiative unsteady flamelet in LES context [23]. Under high-pressure lean-premixed conditions, this study considers into two pathways, namely slow thermal-NO pathway and fast-NO pathway via the steady flamelets. Furthermore, considering the GRI 3.0 mechanism involving all reaction steps for three NO formation mechanisms, the fast-NO pathway is modeled by the NO reaction rate, while the slow thermal-NO is modeled by the extended Zeldovich mechanism.

Fig. 2 shows distributions of reaction-rates for the two NO formation pathways of adiabatic laminar premixed flames for three pressures (p_0=1, 5, 10 bar; ϕ=0.5, T_0=673 K). By increasing pressure, the reaction-rates near the flame front are substantially increased, compared with those of thermal-NO. This implies that the fast-NO pathway could be a dominant pathway at the reaction front of pressurized lean-premixed flames.

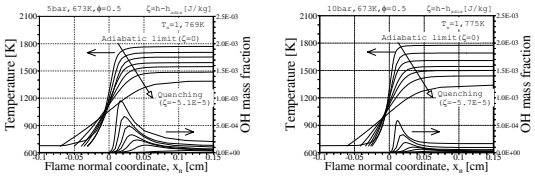

Fig. 1. 1-D laminar premixed CH_4/air flames with heat losses for two pressures (ϕ=0.5, T_0=673 K). (Left) 5 bar, (right) 10 bar.

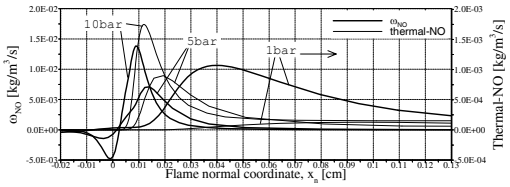

Fig. 2. Comparison of reaction rates for the fast and slow NO formations of 1-D laminar premixed CH_4/air flames for three pressures at adiabatic condition (ϕ=0.5, T_0=673 K).

The instantaneous reaction rates of thermal-NO and NO are also stored as a part of the steady flamelet library. The Favre-mean mass fraction of NO can be determined through a post-processing step where the following transport equation is solved with a time-averaged formation rate:

$$\frac{\partial(\bar{\rho}\tilde{Y}_{\mathrm{NO}})}{\partial t}+\nabla\bullet(\bar{\rho}\,\tilde{u}\,\tilde{Y}_{\mathrm{NO}})=\nabla\bullet(\frac{\mu_T}{S_C}\nabla\tilde{Y}_{\mathrm{NO}})+\overline{\omega_{\mathrm{NO}}} \tag{16}$$

Here the Schmidt number is *S*c=0.7 and the mean reaction rate is calculated using the fast and slow reactions as

$$\begin{aligned}\overline{\omega_{\mathrm{NO}}}(x)=&\int_{-\infty}^{0}\int_{0}^{+\infty}\int_{-\infty}^{+\infty}\omega_{\mathrm{NO,s}}(x_n,\phi,\zeta)P(x_n,\phi,\zeta;x)\mathrm{d}x_n\mathrm{d}\phi\mathrm{d}\zeta\\&+\int_{-\infty}^{0}\int_{0}^{+\infty}\int_{-\infty}^{+\infty}\omega_{\mathrm{NO,f}}(x_n,\phi,\zeta)P(x_n,\phi,\zeta;x)\mathrm{d}x_n\mathrm{d}\phi\mathrm{d}\zeta\end{aligned} \tag{17}$$

where $\omega_{\mathrm{NO,s}}$ denotes for the Zeldovich mechanism and $\omega_{\mathrm{NO,f}}$ for the fast-NO pathway.

2.5 Reinitialization of G-field

The level-set method [13] is quite efficient and robust to track the motion of interface for the object of interest. In this turbulent flame calculation, the $\tilde{G}$-equation is used to determine the mean flame surface $\tilde{G}$ (x,t)=G_0, i.e., zero level-set, because the turbulent burning velocity s_T is defined at the mean flame front only. To avoid numerical difficulties associated with tracking this evolving interface, the scalar G outside G_0 is defined as a signed distance function. This distance function can be obtained using the so-called reinitialization, a numerical technique which satisfies an ansatz $|\nabla G|$=1 outside the zero level-set. The present approach employs a method proposed by Sussman and Fatemi [24], which is required to solve the following Hamilton-Jacobi Eq. [13]:

$$\begin{aligned}&\frac{\partial g}{\partial t}+\mathrm{sign}(g_0)(|\nabla g|-1)=0\ \ \text{with}\\&\quad g(x,0)=g_0(x)=\tilde{G}(x,t)-G_0\end{aligned} \tag{18}$$

or in discretized form:

$$g^{n+1}=g^n-\Delta t\ \mathrm{sign}(g_0)(|\nabla g^n|-1) \tag{19}$$

where the superscript n is the pseudo-time-marching number, Δt is the timestep size (usually less than, or equal to the flow time scale), and sign(g_0) is the sign function. The pseudo-time-marching step is repeated for about 50-200 times, dependent on case by case. From a numerical viewpoint, the reinitialization is a very time-consuming procedure, comparable to the cost for pressure-correction or pdf-integral although considering its important and unavoidable role in the level-set approach. The detailed formulations in context with the unstructured-grid FVM are well described in Refs. [24, 25]. Further details on the present pressure-based unstructured-grid finite-volume method can be found in our previous work [26] and references therein.

3. Results and discussions

The level-set approach in the context of parallel unstructured-grid FVM has been applied to numerically analyze the structure of atmospheric [8] and high-pressure [9] turbulent premixed Bunsen flames. Table 1 summarizes combustion conditions and characteristic parameters averaged at the centerline mean flame front of all investigated flames, where the turbulent Reynolds number, the Damköhler number, and the Karlovitz number are defined as [3]

$$\begin{aligned}&\mathrm{Re}=\left(\frac{u'}{s_L}\right)\left(\frac{l}{l_F}\right),\ \mathrm{Da}=\left(\frac{u'}{s_L}\right)^{-1}\left(\frac{l}{l_F}\right),\\&\mathrm{Ka}^2=\left(\frac{u'}{s_L}\right)^{3}\left(\frac{l}{l_F}\right)^{-1}\end{aligned} \tag{20}$$

Inlet turbulence quantities are determined similarly to Eq. (6) by

$$\tilde{k}=\frac{3}{2}u',\ \ \tilde{\varepsilon}=c_\mu^{3/4}\frac{k^{3/2}}{l}\ \ \text{with}\ c_\mu=0.09 \tag{21}$$

Here the velocity fluctuation is given according to the

Table 1. Combustion conditions and characteristic parameters averaged at the centerline flame front ($|G\text{-}G_0| < 10$ mm, r=0).

Combustion conditions						characteristic parameters				
T_0 (K)	u_0 (m/s)	p_0 (bar)	ϕ	s_L (cm/s)	l_F (mm)	u'/s_L	l/l_F	Re	Da	Ka
298	6	1	0.63	14.39	0.48	4.8	8.1	38.8	1.7	3.7
-	-	-	0.71	21.25	0.33	3.6	13.1	47.1	3.6	1.9
-	-	-	0.83	31.36	0.22	2.2	16.5	36.3	7.5	0.8
673	45	1	0.50	61.20	0.23	8.6	39.0	335.4	4.5	4.0
-	-	5	-	23.93	0.12	22.0	78.0	1716.0	3.5	11.7
-	-	10	-	15.85	0.09	35.8	100.0	3580.0	2.8	21.4
673	30	5	0.43	14.02	0.20	25.8	45.5	1173.9	1.8	19.4
-	-	-	0.50	23.93	0.12	14.9	76.5	1139.8	5.1	6.6
-	-	-	0.56	34.53	0.08	10.1	109.0	1100.9	10.8	3.1

experiments [8, 9] and the length scale is based on the turbulence-grid hole diameter, d_H (i.e., atmospheric Bunsen: u'/u_0=12 %, l=6 mm; high-pressure Bunsen: u'/u_0=5-15 %, l=3 mm; u_0=inlet bulk velocity). Cold flow calculations begin first and then an ignition of mixture follows via an initial G-field with a 20-mm radius ignition core r_0 at x_0=30 mm downstream of the burner exit, i.e. given as $G=r_0-|\mathbf{x}-\mathbf{x}_0|$. This ignition core resembles the small blunt body used as a lighting source in the experiment. After ignition, the flame front propagated until it finally reached a stationary condition.

3.1 Turbulent atmospheric premixed flames

Herrmann et al. [8] experimentally investigated the NO formation characteristics of turbulent premixed methane/air flames at atmospheric pressure for various equivalence ratios and inflow conditions. The experimental setup consists of a concentric Bunsen-type burner with a nozzle diameter d=30 mm and thirty-six pilots with 2-mm diameter. The turbulent premixed flame was stabilized by a ring of small stoichiometric methane pilot flames around the nozzle exit. This burner is operated for a wide range of inflow turbulence conditions using different perforated turbulence-generating grids. Inlet temperature T_0 is fixed at 298 K. Experimental results indicate that the turbulence grid influences the flow field close to the nozzle exit and leads to a nearly homogenous turbulence conditions at the upstream region of the flame tip.

Preliminary calculations have been performed against the various experimental conditions of equivalence ratios (ϕ=1.0, 0.91, 0.83, 0.71, 0.63), turbulence

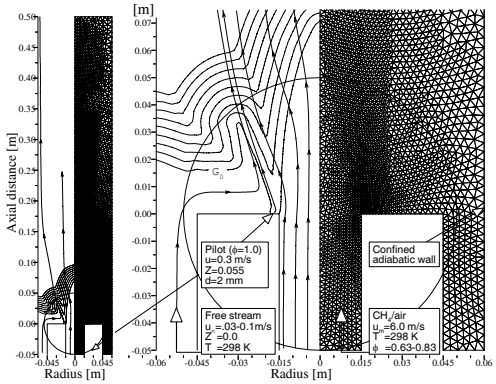

Fig. 3. Problem configuration and unstructured-grid arrangement for turbulent premixed methane/air flames (u_0=6 m/s, T_0=298 K, d=30 mm). G-field and streamlines correspond to ϕ=0.83.

intensities (u'/u_0=6.3-19 %, measured at 10 mm above the nozzle exit), and inlet velocities (u_0=4.5-9.0 m/s). Among the flames, the flame (G16_50) with a given turbulence grid (blockage ratio 50 %, hole diameter 6 mm, position depth 50 mm) is selected as a test case. As shown in Fig. 3, the computational domain comprising 8,957-triangular cells, extends to x=0.5 m downstream of the nozzle exit and r=0.06 m in the radial direction. Corresponding to the turbulence-grid position, incoming mixture is specified at 50 mm below the nozzle exit. A velocity of 0.3 m/s is assumed for the pilot and the entrainment of air is modeled by a velocity varying from 0.03 to 0.1 m/s. The inlet bulk velocity is u_0=6.0 m/s and the measured turbulence intensity of 7 % at x=10 mm, is assumed to be 12 % at the turbulence-grid position.

Fig. 4 shows the flame regimes of three flames (ϕ=0.83, 0.71, 0.63) in terms of the characteristic velocity ratio (u'/s_L) and the length scale ratio (l/l_F) estimated at the centerline mean flame front ($|G\text{-}G_0| <$ 10 mm, r=0). At the flame zones of three atmospheric lean-premixed flames, Damköhler numbers are much larger than 1.0 and Karlovitz numbers are less than 4.0. Among three equivalence ratios, the highest equivalence ratio of 0.83 corresponds to the smallest Ka, 0.8 and the largest Da, 7.5, and the lowest equivalence ratio of 0.63 yields the largest Ka, 3.7 and the smallest Da, 1.7 (see also Table 1). Thus, these three turbulent premixed flames belong to the regimes of both corrugated flamelets and thin reaction zones. These estimated data also indicate that Karlovitz number is substantially decreased with increasing the equivalence ratio and the Damköhler number is sensitively increased with the equivalence ratio.

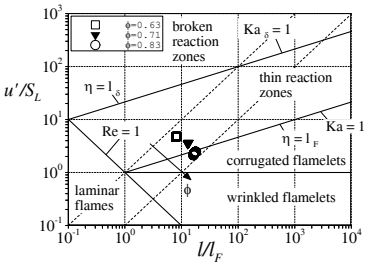

Fig. 4. Borghi diagram and flame regimes of three premixed CH_4/air flames estimated at the centerline, mean flame front ($|G\text{-}G_0|$ < 10 mm, r=0; 3.7 > Ka (ϕ) > 0.8). Kolmogorov length scale (η), inner layer thickness (l_δ), nondimensional thickness of the inner layer (δ).

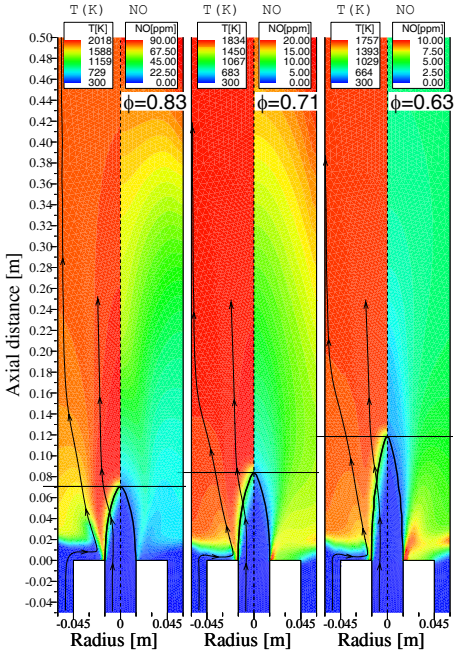

Fig. 5. Mean contours of temperature (K) and NO concentration (ppm) for three equivalence ratios (u_0=6 m/s, T_0=298 K, p_0=1 bar). Curves depict the mean flame front G_0.

Fig. 5 shows the mean contours of temperature and NO concentration for three equivalence ratios (ϕ=0.83, 0.71, 0.63). As shown in Fig. 5, by decreasing the equivalence ratio from 0.83 to 0.63, the mean flame front position moves to the further downstream region. This is mainly due to the decreased Damköhler number, the increased Karlovitz number and the reduced flame temperature which leads to a decrease of both the reaction rate and the turbulent flame speed.

The predicted mean flame front heights for different equivalence ratios are compared with measurements in Fig. 6. These results indicate that the

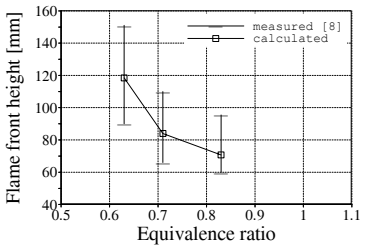

Fig. 6. Comparison of calculated mean flame front height (x=G_0) with measured limits of flame front fluctuation at the centerline for three equivalence ratios.

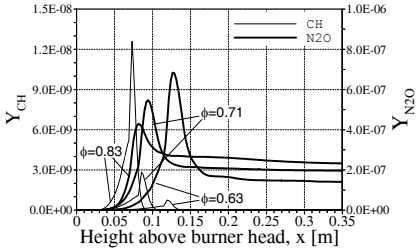

(a) Mass fractions of CH and N2O

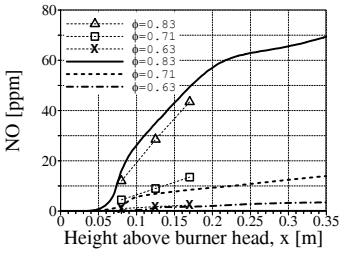

(b) NO concentration

Fig. 7. Centerline profiles of CH, N2O, and NO concentrations for three equivalence ratios. Symbols: experimental measurement [8]; lines: calculation.

predicted data are within the flame front fluctuation limits. Fig. 7 shows the centerline profiles of CH, N2O, and NO concentration for three equivalence ratios (ϕ=0.83, 0.71, 0.63). It can be clearly seen that the NO concentration is substantially decreased by reducing the equivalence ratio. Around the reaction front of the much leaner flame at ϕ=0.63, the N2O mechanism is more dominant than the prompt-NO mechanism. At the post flame zone, the thermal-NO mechanism becomes important. Consequently, the NO level is gradually increased from the flame front to the downstream region. The contribution of thermal-NO at the post flame zone is significantly reduced by decreasing the equivalence ratio. In case of ϕ=0.83, the predicted profile agrees well with the

experimental data. However, for much leaner mixtures (ϕ=0.71, 0.63), there exist certain deviations between predictions and measurements. This discrepancy could be mainly attributed to the shortcomings of the NOx chemistry in the lean-premixed flame situations.

3.2 Turbulent high-pressure lean-premixed flames

Griebel et al. [9] experimentally investigated the flame structure and NOx formation characteristics of turbulent high-pressure lean-premixed methane/air flames. Measurements were made for various pressures, equivalence ratios, and inflow turbulence. This high-pressure combustion rig consists of a concentric Bunsen-type burner with a nozzle diameter d=25 mm and a combustor liner of two coaxial quartz tubes with inner diameter, 75 mm. The methane and combustion air are mixed homogeneously and fed into a generic combustor. The flame is stabilized through the transportation of recirculating hot-burned gas, instead of a pilot flame. The operating temperature T_0 is fixed at 673 K and the pressure ranges from 1 to 10 bar.

The computational domain comprising 7,522-triangular cells, as shown in Fig. 8, extends to x=0.4 m downstream of the nozzle exit and r=0.0375 m in the radial direction. Corresponding to the turbulence grid position, mixture is specified at x=-0.03 m, i.e., 10 times the turbulence-grid hole diameter d_H=3 mm, below the nozzle exit. To account for the convective air-cooling effect on the combustor liner, a fixed wall temperature is imposed along the liner. Computations are carried out, respectively, for six flames at three pressures (p_0=1, 5, 10 bar; ϕ=0.5, u_0=45 m/s) and three equivalence ratios (ϕ=0.43, 0.50, 0.56; p_0=5 bar, u_0=30 m/s). These experimental conditions for high-pressure lean-premixed flames are quite similar to the operating conditions of the lean-premixed gas turbine combustors in terms of pressure, temperature, and equivalence ratio.

For these flames, Griebel et al. [9] assumed the inlet turbulence intensity (u') to be 10 % of the bulk velocity and approximated the inlet integral length scale (l) by the turbulence-grid hole diameter. Accordingly, here u' is adjusted and l is given by the hole diameter d_H=3 mm. Due to lack of the liner temperature, we assume a wall temperature of T_w=1,450 K throughout calculations, consistently except for 1-bar case where a higher relative heat loss is expected due to the lower thermal loading. Table 2 summarizes the boundary conditions and the calculated mean flame characteristics including flame front height (x_f), and NO concentration and temperature at the combustor exit, x=0.39 m.

Table 2. Boundary conditions and calculated flame characteristics (d=25 mm, T_0=673 K).

ϕ	p_0 (bar)	u_0 (m/s)	u'/u_0 (%)	T_w (K)	x_f/d	NO_{exit} (ppm)	T_{exit} (K)
0.50	1	45	5	450	7.24	1.81	1,468
-	5	-	12	1,450	6.84	1.90	1,618
-	10	-	15	1,450	6.56	1.22	1,626
0.43	5	30	12	1,450	7.36	0.37	1,459
0.50	-	-	12	1,450	6.28	1.56	1,561
0.56	-	-	12	1,450	4.72	4.29	1,643

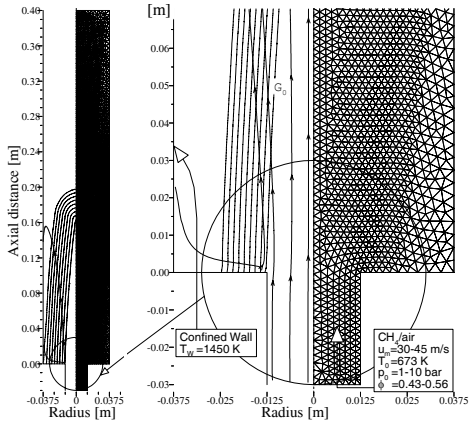

Fig. 8. Problem configuration and unstructured-grid arrangement for turbulent high-pressure lean-premixed methane/air flames (T_0=673 K, d=25 mm, D=75 mm). G-field and streamlines correspond to ϕ=0.5 and 10 bar.

Fig. 9 shows the flame regimes of the investigated flames in terms of u'/s_L and l/l_F estimated at the centerline mean flame front ($|G-G_0|$ < 10 mm, r=0). The results describe well that Karlovitz number increases with increasing the pressure and decreases with increasing the equivalence ratio. Numerical results indicate that these premixed flames are located well within the thin reaction zones regime as described in the experiment [9].

Fig. 10 shows the mean contours of temperature and NO concentration for three pressures (p_0=1, 5, 10 bar; ϕ=0.5, u_0=45 m/s). At the flame zone, the non-dimensional parameters corresponding to the relatively low-pressure case of 1 bar are roughly estimated as Re=335, Da=4.5, and Ka=4.0, and those corresponding to the relatively high-pressure case of 10 bar are also given as Re=3,580, Da=2.8, and

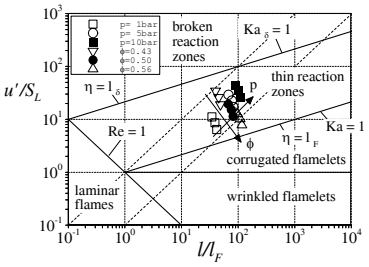

Fig. 9. Borghi diagram and flame regimes of six premixed CH_4/air flames estimated at the centerline, mean flame front ($|G\text{-}G_0|$ < 10 mm, r=0; 4.0 < Ka (p) < 21.4, 19.4 > Ka (ϕ) > 3.1).

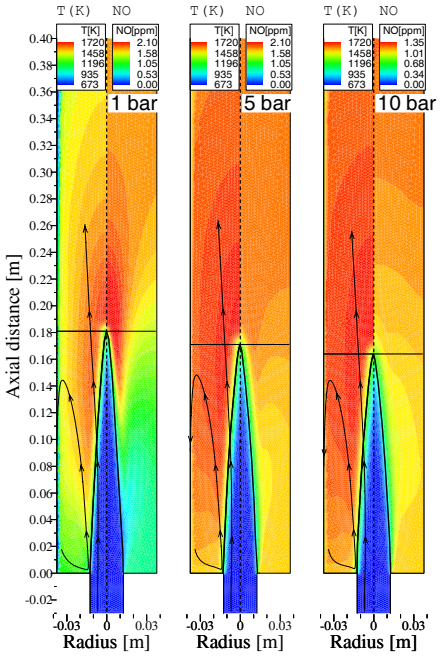

Fig. 10. Mean contours of temperature (K) and NO concentration (ppm) for three pressures (ϕ=0.5, u_0=45 m/s, T_0=673 K). Curves depict the mean flame front G_0.

Ka=21.4. Thus, these three turbulent premixed flames belong to the thin reaction zones (see also Fig. 9). These estimated data also indicate that the turbulent Reynolds number and Karlovitz number are sensitively increased with the pressure, and the Damköhler number is marginally decreased with the pressure.

As shown in Fig. 10, by increasing the pressure from 1 to 10 bar the mean flame front position slightly moves to the upstream region. The increased pressure corresponds to the elevated turbulent Reynolds number, which results in the increase of the turbulent flame speed through the enhanced flame

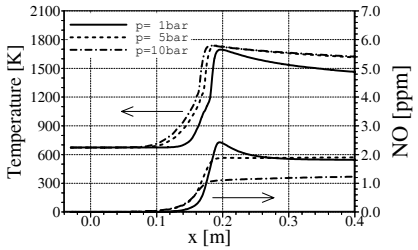

Fig. 11. Centerline profiles of mean temperature and NO concentration for three pressures (ϕ=0.5, u_0=45 m/s, T_0=673 K).

corrugation. Even if the laminar flame speed considerably decreases with the pressure, the turbulent flame speed still increases with the pressure because the enhanced flame corrugation is more dominant than the effect of laminar flame speed on the turbulent flame speed. This trend is well explained in the measurements. The predicted contours of NO concentration agree qualitatively with the measured image of NO-LIF [9].

Fig. 11 shows the centerline profiles of mean temperature and NO concentration for three pressures (p_0=1, 5, 10 bar). Increasing the pressure causes the NO concentration to increase due to the higher burnt gas temperatures. These higher temperatures are caused by the higher thermal power at higher pressure, compared to the relative heat loss. However, at the pressure of 10 bar, the NO concentration decreases. Griebel et al. [9] mentioned that, at the high-pressure combustion conditions, the decrease of NO concentration could be mainly caused by the lower concentration of radical pool including OH and O. As shown in Fig. 1, this trend can be seen from the distributions of OH radical at pressures of 5 and 10 bar. In addition, it can be assumed that, under similar temperature at higher pressures, the reduced flame brush thickness can result in a decrease of the NO formation due to the fast-NO mechanism as shown in Fig. 2. This typical behavior at higher pressures is well reproduced by the present approach.

Fig. 12 shows the mean contours of temperature and NO concentration for three equivalence ratios (ϕ=0.43, 0.5, 0.56; p_0=5 bar, u_0=30 m/s). At the flame zone, the non-dimensional parameters corresponding to the relatively low equivalence ratio of 0.43 are roughly estimated as Re=1,173, Da=1.8, and Ka=19.4 and those corresponding to the relatively high equivalence ratio of 0.56 are also given as Re=1,100, Da=10.8, and Ka=3.1. Again, these three turbulent

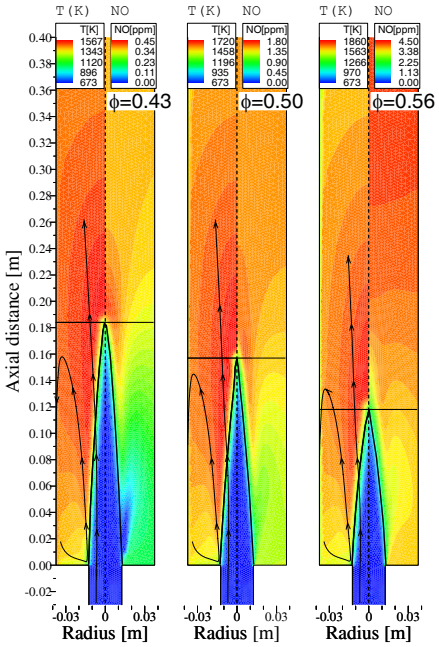

Fig. 12. Mean contours of temperature (K) and NO concentration (ppm) for three equivalence ratios (p_0=5 bar, u_0=30 m/s, T_0=673 K). Curves depict the mean flame front G_0.

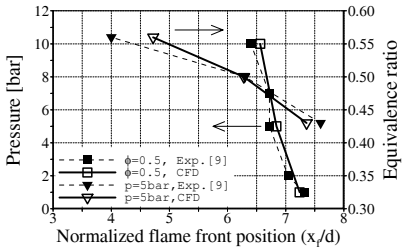

Fig. 13. Comparison of calculated mean flame front position (x=G_0) with measurement (x_{mean}) at the centerline for different pressures and equivalence ratios (p_0=1, 5, 10 bar; ϕ=0.43, 0.5, 0.56; T_0=673 K, d=25 mm).

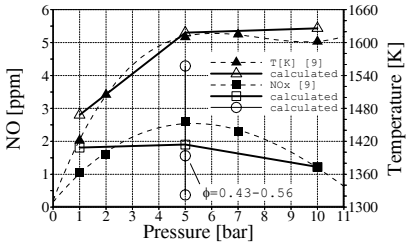

Fig. 14. Comparison of NO concentration and mean temperature at the combustor exit of x=0.39 m for different pressures (ϕ=0.5, u_0=45 m/s, T_0=673 K).

premixed flames belong to the thin reaction zones (see also Fig. 9). These estimated data also indicate that Karlovitz number is substantially decreased with the equivalence ratio and the Damköhler number is sensitively increased with the equivalence ratio. However, it is also found that the turbulent Reynolds number is almost independent of the equivalence ratio.

As shown in Fig. 12, by decreasing the equivalence ratio from 0.56 to 0.43, the mean flame front position moves to the further downstream region. This is mainly due to the decreased Damköhler number, the increased Karlovitz number and the reduced flame temperature which results in decreasing the reaction rate and the turbulent flame speed.

Fig. 13 compares the mean flame front heights for different pressures and equivalence ratios. The overall agreement with measurements is good. Increasing the pressure leads to a slight decrease of the flame heights due to increased turbulent flame speed caused by the elevated turbulence intensity through the enhanced flame corrugation. Increasing the equivalence ratio causes a decrease of the flame heights due to the increased flame temperature leading to a higher reaction rate and turbulent flame speed.

In Fig. 14 the mean temperature and NO concentration at the combustor exit of x=0.39 m for different pressures at ϕ=0.5 is compared with measurements. Apart from the convective heat transfer at the wall, the radiation effect results in a further decrease of temperature about 70-140 K at the combustor exit. The experimental data reveals slight fluctuations at higher pressures, which are not shown here. Although some discrepancies exist, the agreement is reasonably good. The discrepancies could be attributed mainly to the uncertainties in the imposition of the wall boundary condition for heat losses as well as marginally to the limitation of the present turbulent combustion model. In addition to the pressure variations, the predicted NO concentration for different equivalence ratios is also presented in Fig. 14. The NO concentration is substantially decreased from 4.3 to 0.4 ppm by reducing the equivalence ratio from 0.56 to 0.43. These numerical results suggest that the NO emission level of a lean-premixed gas turbine combustor (ϕ < 0.5) could be less than 10 ppm if the perfectly premixed mixtures are supplied.

4. Conclusions

Numerical results obtained in this study suggest that the flamelet model based on the level-set approach in the context of parallel unstructured-grid

finite-volume method is capable of realistically simulating the detailed structure and NO formation in the atmospheric and high-pressure lean-premixed flames. Based on the numerical results, the following conclusions can be drawn:

(1) For atmospheric and high-pressure lean-premixed flames, by decreasing the equivalence ratio from 0.83 to 0.63, the mean flame front position moves to the further downstream region. This is mainly due to the decreased Damköhler number, the increased Karlovitz number, and the reduced flame temperature which leads to decrease the reaction rate and the turbulent flame speed. The flame heights for different equivalence ratios agree with measurements.

(2) The NO concentration is substantially decreased by reducing the equivalence ratio. Around at the reaction front of the much leaner flames (ϕ=0.63), the N2O mechanism is more dominant than the prompt-NO mechanism. Due to the thermal-NO mechanism becoming important, the NO level is gradually increased from the flame front to the downstream region. For ϕ=0.83, the predicted profile agrees well with the experimental data. However, for the much leaner mixtures (ϕ=0.71 and 0.63), there exist certain deviations between predictions and measurements.

(3) For turbulent high-pressure lean-premixed flames, the estimated non-dimensional parameters indicate that the turbulent Reynolds number and Karlovitz number are sensitively increased with the pressure, and the Damköhler number is marginally decreased with the pressure. The increased pressure corresponds to the elevated turbulent Reynolds number, which results in the increase of the turbulent flame speed through the enhanced flame corrugation.

(4) By decreasing the equivalence ratio from 0.56 to 0.43 at 5 bar, the mean flame front position moves to the further downstream region. This is mainly due to the decreased Damköhler number, the increased Karlovitz number, and the reduced flame temperature, which leads to decrease the reaction rate and the turbulent flame speed.

(5) At the high-pressure and high-temperature lean-premixed turbulent flames, numerical results indicate that the flame heights for different pressures and equivalence ratios are reasonably well predicted. The NO concentration is substantially decreased by reducing the equivalence ratio from 0.56 to 0.43. The predicted NO emission levels for three equivalence ratios are less than 4.3 ppm. These numerical results suggest that the NO emission level of a lean-premixed gas turbine combustor (ϕ < 0.5) could be less than 10 ppm if the perfectly premixed mixtures are supplied.

Acknowledgment

This research was supported by Grant AE2-101-1-0-1 from the Carbon Dioxide Reduction & Sequestration Research Center, one of the 21st Century Frontier Programs funded by the Ministry of Science and Technology of the Korean Government.

References

[1] R. Borghi, On the structure and morphology of premixed flames, in: *Recent Advances in the Aerospace Science*, C. Casci, Ed., Plenum Press, New York, (1985) 117-138.

[2] N. Peters, The turbulent burning velocity for large-scale and small-scale turbulence, *J. Fluid Mech*., 384 (1999) 107-132.

[3] N. Peters, *Turbulent Combustion*, Cambridge University Press, Cambridge, UK, (2000).

[4] A. Y. Klimenko and R. W. Bilger, Conditional moment closure for turbulent combustion, *Prog. Energy Combust. Sci*., 25 (1999) 595-687.

[5] D. Bradley, P. H. Gaskell and A. K. C. Lau, A mixedness-reactedness flamelet model for turbulent diffusion flames, *23rd Symp.* (*Int.*) *on Combustion*, (1990) 685-692.

[6] V. L. Zimont, F. Biagioli and K. Syed, Modelling turbulent premixed combustion in the intermediate steady propagation regime, *Int. J. Progress in Computational Fluid Dynamics*, 1 (2001) 14-28.

[7] M. Chen, M. G. Herrmann and N. Peters, Flamelet modeling of lifted turbulent methane/air and propane/air jet diffusion flames, *28th Symp*. (*Int.*) *on Combustion*, (2000) 167-174.

[8] K. Herrmann and K. Boulouchos, Nitric oxide detection in turbulent premixed methane/air flames, *Proc. Combust. Inst*., 30 (2005) 1517-1525.

[9] P. Griebel, R. Bombach, A. Inauen, W. Kreutner and R. Schären, Structure and NO emission of turbulent high pressure lean premixed methane/air flames, *Proc. 6th European Conference on Industrial Furnaces and Boilers*, Vol. II, ISBN-972-8034-05-9, INFUB (2002) 45-54.

[10] A. Favre, Statistical Equations of Turbulent Gases, in: *Problems of Hydrodynamics and Continuum Mechanics*, Society for Industrial and Applied Mathematics, Philadelphia, PA, USA, (1969) 231-266.

[11] S. Kang and Y. Kim, Parallel unstructured-grid finite-volume method for turbulent nonpremixed flames using the flamelet model, *Numer. Heat Transfer, Part B*, 43 (2003) 525-547.

[12] The International Workshop on Measurement and Computation of Turbulent Nonpremixed Flames (TNF) (available at URL: http://www.ca.sandia.gov/TNF/)

[13] J. A. Sethian, *Level Set Methods and Fast Marching Methods*, 2nd Ed., Cambridge University Press, Cambridge, UK, (1999).

[14] F. A. Williams, Turbulent Combustion, in: *The Mathematics of Combustion*, J. D. Buckmaster, Ed., Society for Industrial and Applied Mathematics, Philadelphia, PA, USA, (1985) 97-131.

[15] S. B. Pope, Pdf methods for turbulent reactive flows, *Prog. Energy Combust. Sci.*, 11 (1985) 119-192.

[16] N. Peters, Laminar diffusion flamelet models in non-premixed turbulent combustion, *Prog. Energy Combust. Sci*., 10 (1984) 319-339.

[17] M. G. Herrmann, Numerical Simulation of Premixed Turbulent Combustion Based on a Level Set Flamelet Model. Ph.D. Thesis, RWTH Aachen, (2001).

[18] C. M. Müller, H. Breitbach and N. Peters, Partially premixed turbulent flame propagation in jet flames, *25th Symp.* (*Int.*) *on Combustion*, (1994) 1099-1106.

[19] J. C. Ferreira, Flamelet Modelling of Stabilization in Turbulent Non-premixed Combustion, Ph.D. Thesis, ETH-Zuerich Switzerland, (1996).

[20] B. Fiorina, R. Baron, O. Gicquel, D. Thevenin, S. Carpentier and N. Darabiha, Modelling non-adiabatic partially premixed flames using flame-prolongation of ILDM, *Combust. Theory Modelling*, 7 (2003) 449-470.

[21] R. J. Kee, F. M. Rupley and J. A. Miller, CHEMKIN-II: A Fortran Chemical Kinetics Package for the Analysis of Gas Phase Chemical Kinetics, Technical Report SAND89-8009B UC-706, Sandia National Laboratories, USA, (1992).

[22] G. P. Smith, D. M. Golden, M. Frenklach, N. W. Moriarty, B. Eiteneer, M. Goldenberg, C. T. Bowman, R. K. Hanson, S. Song, W. C. Gardiner, Jr., V. V. Lissianski and Z. Qin, *Gri-mech 3.0*, University of California-Berkeley, (1999) http://www.me.berkeley.edu/gri_mech/.

[23] M. Ihme and H. Pitsch, Modeling of radiation and nitric oxide formation in turbulent nonpremixed flames using a flamelet/progress variable formulation, *Phys. Fluids*, 20, 055110 (2008) 1-20.

[24] M. Sussman and E. Fatemi, Level set redistancing algorithm, *SIAM J. Sci. Comput*., 20 (4) (1999) 1165-1191.

[25] S. Kang, H. Kim, Y. Kim and K.-Y. Ahn, Level-set based flamelet approach for simulating turbulent lifted jet flame, *Int. J. Numer. Meth. Fluids*, 58 (2008) 573-589.

[26] S. Kang and Y. Kim, Pressure-based unstructured-grid finite-volume method for simulating laminar reacting flows, *Numer. Heat Transfer, Part B*, 41 (2002) 53-72.

Sungmo Kang received his B.S. in Mechanical Engineering from Hanyang University, Korea, in 1993. He then received his M.S. and Ph.D. degrees from Hanyang University in 1996 and 2002, respectively. Dr. Kang is currently a research associate in the Department of Mechanical Engineering at Hanyang University in Seoul, Korea. His primary research interest is the parallel unstructured-grid method, numerical and physical modeling for chemically reacting flows and pollutant formation in combustion processes.

Yongmo Kim received his B.S. in Mechanical Engineering from Hanyang University, Korea, in 1976. He then received his Ph.D. degree from University of Alabama in Huntsville in 1987. Dr. Kim is currently a professor in the Department of Mechanical Engineering at Hanyang University in Seoul, Korea. His research interest is combustion modeling.